

# Contrastive Learning for Lane Detection via Cross-Cimilarity

Ali Zoljodi<sup>1</sup>, Sadegh Abadijoui<sup>2</sup>, Mina Alibeigi<sup>3</sup>, Masoud Daneshtalab<sup>1</sup>

<sup>1</sup>Mälardalen University

<sup>2</sup>University of Leicester

<sup>3</sup>Zenseact AB

ali.zoljodi@mdu.se, ma1023@leicester.ac.uk, mina.alibeigi@zenseact.com, masoud.daneshtalab@mdu.se

## Abstract

Detecting road lanes is challenging due to intricate markings vulnerable to unfavorable conditions. Lane markings have strong shape priors, but their visibility is easily compromised. Factors like lighting, weather, vehicles, pedestrians, and aging colors challenge the detection. A large amount of data is required to train a lane detection approach that can withstand natural variations caused by low visibility. This is because there are numerous lane shapes and natural variations that exist. Our solution, Contrastive Learning for Lane Detection via cross-similarity (CLLD), is a self-supervised learning method that tackles this challenge by enhancing lane detection models' resilience to real-world conditions that cause lane low visibility. CLLD is a novel multitask contrastive learning that trains lane detection approaches to detect lane markings even in low visible situations by integrating local feature contrastive learning (CL) with our new proposed operation *cross-similarity*. Local feature CL focuses on extracting features for small image parts, which is necessary to localize lane segments, while cross-similarity captures global features to detect obscured lane segments using their surrounding. We enhance cross-similarity by randomly masking parts of input images for augmentation. Evaluated on benchmark datasets, CLLD outperforms state-of-the-art contrastive learning, especially in visibility-impairing conditions like shadows. Compared to supervised learning, CLLD excels in scenarios such as shadows and crowded scenes.

## Introduction

Lane detection is a challenging task in the real world due to the properties of lane markings. Lane markings are long, thin structures with strong shape priors (Pan et al. 2018). Natural variations such as poor lighting, frequent occlusion, and other environmental disturbances significantly reduce their visibility, leading to a high risk of not being detected by machines (Liu et al. 2021). A robust lane detection model must capture spatial information to detect poorly visible parts of lanes using other areas that are more visible (Pan et al. 2018). Many novel lane detection approaches employ pixel-level image segmentation techniques (Zheng et al. 2021; Pan et al. 2018; Moujtahid et al. 2022) to enhance the precision of lane detection. In this group of methods, each pixel is labeled as belonging either to a lane or the background.

To develop a reliable lane detection method that can handle natural variations, a significant amount of training data

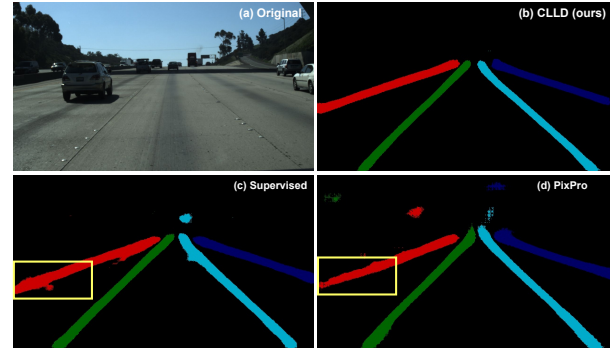


Figure 1: Comparison between the output of state-of-the-art segmentation-based lane detection RESA (Zheng et al. 2021) with three different pretraining strategy. (a) The input (b) RESA output with CLLD (ours) pretraining (c) RESA output with supervised pretraining (d) RESA output with PixPro (Xie et al. 2021) pretraining.

is required. Obtaining enough labeled data for lane detection requires a huge amount of human labor. Furthermore, the appearance of lanes varies across the globe. Unsupervised and self-supervised *contrastive learning* (CL) methods have been proposed for training *deep neural networks* (DNNs) with minimal labeled data and a vast amount of unlabeled data (Chen et al. 2020a; Bardes, Ponce, and LeCun 2021; He et al. 2020; Chen and He 2021; Xie et al. 2021; Bardes, Ponce, and LeCun 2022; Wang et al. 2021). Based on their application, CLs are divided into *global feature* CLs and *local feature* CLs. When it comes to lane detection, using global feature CLs for image classification is not the most effective approach. This is because global feature CLs contrast an entire input image to other images, whereas lane detection requires localizing specific lane segments by contrasting different segments of the same input image. These models are intended to identify useful features for detecting the object present in the input rather than pinpointing its location on the input. Local feature CL is proposed to explicitly learn features that classify small parts of the input (Bardes, Ponce, and LeCun 2022). They can be used for object localization approaches such as lane detection.

Existing local feature CLs are not adequate for lane de-

tection. They are designed to detect completely visible objects and do not have any mechanism to predict the existence of objects which are obscured due to natural variations. To effectively detect and pinpoint lane markings, even in low visibility areas, we propose to use *contrastive learning for lane detection via cross-similarity* (CLLD), a self-supervised learning method for lane detection. CLLD is a multi-task contrastive learning approach. It trains *convolutional neural networks* CNNs to segment an input image. Plus, it trains CNNs to predict masked parts of an image using their surrounding parts. In order to train the segmentation, we provided both an input image and its augmented version to an encoder. We then measured the consistency between the original image’s feature map and the feature map generated from the augmented version that warped to its original shape. Our augmentation includes image masking. It is a necessary augmentation for training the CNN to predict missed data using its surrounding available data (He et al. 2022). However, we are unable to compare the feature map of the masked area with its corresponding feature map on the original image. To overcome this challenge, we utilized the similarity of the feature maps surrounding the masked area with its corresponding feature map in the original image’s feature map by proposing our new operation *cross-similarity*. We compute the cross-similarity of every patch of the feature map in the masked image with all parts of the feature map in the original image and contrast it with the cross-similarity of every patch in the original image feature maps and the entire masked image features map. This trains the CNN to predict masked parts using its surrounding. To the best of our knowledge, CLLD is the first contrastive learning method that predicts local features for obscured parts of the objects using their surrounding.

We assess CLLD on U-Net (Ronneberger, Fischer, and Brox 2015), a popular encoder-decoder which widely utilized in lane detection algorithms (Lee and Liu 2022; Zou et al. 2019; Tran and Le 2019a; Moujtahid et al. 2022). In addition to U-Net, we evaluate the proposed method on *Recurrent Feature-Shift Aggregator for Lane Detection* (RESA) (Zheng et al. 2021) and *Cross Layer Refinement Network for Lane Detection* (CLRNet) (Zheng et al. 2022) as state-of-the-art segmentation-based and anchor-based lane detection methods, respectively. CLLD yields an average 1% improvement in all accuracy metrics over state-of-the-art contrastive learning methods on two of the most well-known lane detection datasets, CuLane (Pan et al. 2018) and TuSimple (Weng et al. 2021). The CLLD is designed to train lane detection approaches, producing results that are resilient to natural variations. To demonstrate its efficacy, we have tested CLLD on the shadow subset of CuLane, known to be a challenging set due to its varying light conditions. Our findings show an impressive over 4% improvement in detecting lanes within the more difficult shadow subset of CuLane. In the visualized results shown in Figure 1, CLLD outperforms state-of-the-art local feature CL and supervised learning. Specifically, CLLD is more effective at dealing with occluded parts of a lane. Based on the results provided, it is justified that CLLD is more efficient than the current state-of-the-art CL for detecting lanes.

## Related work

### lane detection

Lane detection is a critical module in autonomous vehicles. The safety of autonomous vehicles is greatly affected by the accuracy and latency of lane detection methods. Lane detection methods are classified as conventional (Borkar, Hayes, and Smith 2011; Deusch et al. 2012; Hur, Kang, and Seo 2013; Wu, Chang, and Lin 2014; Sun, Tsai, and Chan 2006; Yu and Jain 1997) or based on CNN (Kim and Lee 2014; Gurghian et al. 2016; Sermanet et al. 2013; Kim and Park 2017; Neven et al. 2018; Pan et al. 2018; Zheng et al. 2021). Conventional lane detection (Sun, Tsai, and Chan 2006; Yu and Jain 1997) relies on manual features to identify lanes, limiting their accuracy in different road conditions.

CNN technology has enabled new solutions for lane detection, such as U-Net (Tran and Le 2019b) and LaneNet (Neven et al. 2018). However, challenges arise when detecting occluded lanes due to biases and spatial information capture limitations. Spatial CNN (Pan et al. 2018) and Recurrent Feature-Shift Aggregator (Zheng et al. 2021) address these challenges by using message-passing to propagate spatial information. Anchor-based (Zheng et al. 2022; Qin, Zhang, and Li 2022) and key point (Wang et al. 2022; Qu et al. 2021; Tabelini et al. 2021) lane detection options are also some lane detection method that behave lane as a chain of anchors and key points, respectively. This paper discusses how CLLD can enhance the accuracy and resilience of segmentation-based and anchor-based lane detection. However, the keypoint lane detection mechanism, which relies on identifying and linking keypoints, cannot take advantage of CLLD to detect any missed sections of lanes.

### contrastive learning

Based on their applications, contrastive learning (CL) methods are divided into *global feature* (Chen et al. 2020a; Bardes, Ponce, and LeCun 2022; Chen, Xie, and He 2021; Wang et al. 2021; Mitrovic et al. 2020; Bardes, Ponce, and LeCun 2021; Mitrovic et al. 2020; He et al. 2020; Chen and He 2021; Henaff 2020; Tian, Krishnan, and Isola 2020) and *local feature* (Wang et al. 2021; Bardes, Ponce, and LeCun 2022; Xie et al. 2021; Zhao et al. 2021; Xiao et al. 2021) CLs.

**global features** Global feature methods can aid in image classification by comparing positive and negative samples. Studies such as (Tian, Krishnan, and Isola 2020), SimCLR (Chen et al. 2020a), and MoCo (He et al. 2020) use different techniques to train the network to produce similar representations for all views of a sample. However, these methods may not work well for identifying specific parts of an image, as noted by (Xie et al. 2021).

**local features** Local features are proposed to overcome pixel-level and region-level classifications. Different levels of local feature methods can be utilized such as at the feature-level (Wang et al. 2021; Bardes, Ponce, and LeCun 2022), pixel-level (Xie et al. 2021; Zhao et al. 2021), or region-level (Xiao et al. 2021). DenseCL (Wang et al. 2021)

is a method that discriminates at the feature-level, inspired by MoCo-V2 (Chen et al. 2020b). PixPro (Xie et al. 2021) is a method that discriminates at the pixel-level, inspired by BYOL (Grill et al. 2020). The positive samples are identified by pixels with Euclidean distance smaller than a threshold. VICRegL (Bardes, Ponce, and LeCun 2022) is a trade-off of global and local features that aims to achieve a balance in representation learning. Detecting obscured lanes can be difficult with local feature CLs as they only extract visible segments. However, our method, CLLD, is capable of not only extracting visible parts of lanes but also predicting the existence of obscured lanes based on their surrounding visible parts.

## Method

Using CLLD, lane detection encoders are learned to reconstruct low visible lane parts by solving Eq. (1).

$$\mathcal{W}^* = \arg \min_{\mathcal{W}} \sum_{p \in P} \mathcal{L}_{clld}(\mathcal{F}(\mathcal{I}_p), \mathcal{F}(\mathcal{M}(\mathcal{I}_p))) \quad (1)$$

The variable  $\mathcal{W}^*$  denotes the optimized weights for the lane detection encoder. And  $\mathcal{I}$  is the input training image. The optimization problem is designed to extract local features. Therefore, the input  $\mathcal{I}$  is divided into  $P$  patches. And the contrastive loss  $\mathcal{L}(\cdot)$  is applied to each patch  $p \in P$ , which is fed two times to the CNN backbone  $\mathcal{F}$ , one time in the original shape  $\mathcal{F}(\mathcal{I}_p)$  and one time in the masked shape  $\mathcal{F}(\mathcal{M}(\mathcal{I}_p))$ . The optimization problem aims to minimize the summation of loss values for all patches  $\sum_{p \in P}(\cdot)$ .

We take lanes as objects with strong shape priors, which follow a solid pattern and may occasionally become invisible in some random parts. Through our empirical studies, we have found that masking certain areas of the input image and training the encoder to predict those specific parts can be a beneficial method for training the lane detection backbone to predict occluded or missing lane segments. As a result, we employ this technique by masking the input image to generate a second view utilized by the contrastive learning method. Below, we will give you a thorough explanation of the masking that we utilized.

Local feature CLs warp applied data augmentations on features to locate corresponding features of corresponding pixels within the original image. When using masking, it is not possible to warp areas that have been masked, as no features are extracted from those sections. Our proposal involves a crucial step to overcome the aforementioned difficulty - improving the extracted feature maps with *cross-similarity* information. This module calculates the similarity between each patch of the feature map from the original image, denoted as  $\mathcal{F}(\mathcal{I}_p)$ , and all patches from the feature map of the masked image, denoted as  $\{\forall p \in P : \mathcal{F}(\mathcal{M}(\mathcal{I}_p))\}$ . It also compares each patch of the feature map from the masked image,  $\mathcal{F}(\mathcal{M}(\mathcal{I}_p))$ , to all patches from the feature map of the original image, denoted as  $\{\forall p \in P : \mathcal{F}(\mathcal{I}_p)\}$ .

Through *cross-similarity*, each patch  $\mathcal{F}(\mathcal{I}_p)$  has the ability to interact with all the patches in the cross-view, thereby maintaining the positional information of the

patches. *cross-similarity* allows for the use of the local feature CL on masked images. This is accomplished by sharing information from each patch with all the other patches in the cross-view, particularly the corresponding patch. Following we provide a comprehensive explanation of the *cross-similarity* concept.

## Contrastive Learning for Lane Detection

Our method (CLLD) is a momentum contrastive learning (Xie et al. 2021; He et al. 2020; Chen et al. 2020b; Wang et al. 2021) (Figure 2). Given the input image  $\mathcal{I}$ , the masking function masks some random patches with the size  $\rho \times \rho$  and produces a masked view of the input  $\mathcal{M}(\mathcal{I})$ . We input  $\mathcal{I}$  and  $\mathcal{M}(\mathcal{I})$  into two different encoders. The first encoder uses gradient descent to update its weights, while the second one updates its weights using the momentum of the first encoder. The output of  $\mathcal{M}(\mathcal{I})$  is a feature map  $\mathcal{F}(\mathcal{M}(\mathcal{I}))$  that may not have valid information for the masked areas. To enhance the masked areas with comparable information, we compute the *cross-similarity* of each patch from  $\mathcal{F}(\mathcal{M}(\mathcal{I}))$  and the entire feature map of the input  $\mathcal{F}(\mathcal{I})$ . We perform the inverse operation on each patch within  $\mathcal{F}(\mathcal{I})$  and the entirety of  $\mathcal{F}(\mathcal{M}(\mathcal{I}))$  (as discussed above).

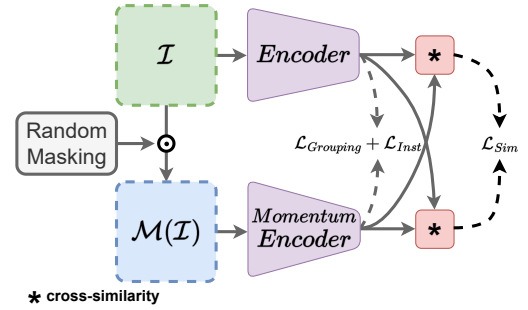


Figure 2: The CLLD framework.

## Masking

In this study, similar to *masked image modeling* approach (Bao et al. 2021), we mask random portions of inputs and train the backbone to predict masked parts. This approach train lane detection backbones to predict hidden objects using their surrounding which is a necessary application for lane detection algorithms in dealing with occluded or vanished lane markings. The random locations are square patches (with size  $\rho \times \rho$ ) of input images. For a given input  $\mathcal{I} \in [0, 1]^{H \times W \times C}$  and portions to mask  $\mathcal{M} = \{[0, 1]^{i \times j}, \text{ where } i \in \{0, H/P\} \text{ and } j \in \{0, W/P\}\}$ , the masked image is generated using Eq. (2).

$$\mathcal{M}(\mathcal{I}) = \begin{cases} \mathcal{N}(0, 1) & \text{if } \mathcal{M} \\ \mathcal{I} & \text{otherwise} \end{cases} \quad (2)$$

Where  $\mathcal{M}(\mathcal{I})$  is the masking image. To replace the pixel value in the masked portion, we randomly select a value from the normal distribution  $\mathcal{N}(0, 1)$ . To avoid biasing the model on a particular masking value, it is advisable to replace it with a random value.

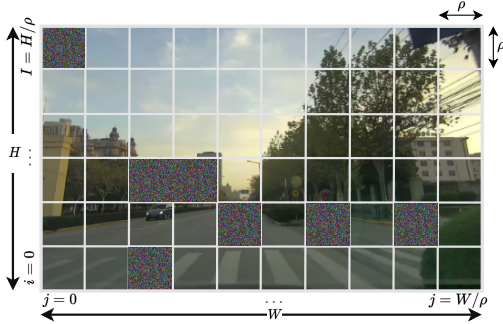


Figure 3: Masking input image; The given input with size  $H \times W$  is divided into  $\rho \times \rho$  patches. Each pixel of the masked patch got a random value from a zero-mean normal distribution  $\mathcal{N}(0, 1)$ .

### cross-similarity

To uncover the local features of masked patches, we utilize the similarity of its surrounding features and its corresponding features in the original image by applying cross-similarity operation (Figure 4).

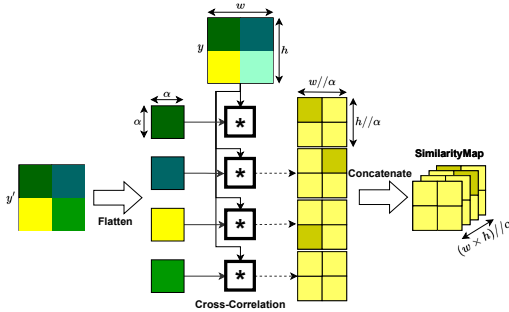


Figure 4: The cross-similarity operation

Assume the output of feeding the original input image  $I$  is  $y$  and the output of feeding masked image  $\mathcal{M}(I)$  is  $y'$ . In order to extract local features, the contrastive loss needs to be applied to the small patches of  $y$  and  $y'$ . These patches are denoted by  $\{y_p$  and  $y'_p, \forall p \in P\}$ , where  $P$  represents all patches within a feature map. The cross-similarity between the full feature map of the first view and a patch of the feature map of the second view  $y'_p$  is calculated through the use of Eq. (3).

$$CS(y, y'_p)[i, j] = \sum_{u=-\frac{\alpha}{2}}^{\frac{\alpha}{2}} \sum_{v=-\frac{\alpha}{2}}^{\frac{\alpha}{2}} y'_p[u, v] y[i+u, j+v] \quad \forall i \in [0, h/\alpha] \text{ and } \forall j \in [0, w/\alpha] \quad (3)$$

The  $\alpha$  represents the measurement of the sides of each patch. And  $h$  and  $w$  denote feature maps' height and width, respectively. To generate the complete cross-similarity between  $y$  and  $y'$ , we compute the cross-similarity be-

tween  $y$  and every patch of  $y'$  ( $\forall p \in y'$ ) and then concatenate them all together (Eq. (4)).

$$CS(y, (\forall p \in y')) = [CS(p_0, y), CS(p_1, y), \dots, CS(p_z, y)] \quad \text{where } z = (w \times h)/\alpha \quad (4)$$

In order to calculate the cross-similarity of  $y$  with  $y'$ , denoted as  $CS(y', (\forall p \in y))$ , we perform the same operation as before but with  $y$  and  $y'$  swapped.

As shown in Figure 4, the cross-similarity of each patch  $y'_p$  with the feature map  $y$  is saved in a separate tensor. These tensors are then concatenated in their respective order. By using this mechanism, one can not only discover the similarity between each patch from one feature map and all patches from the other but also retain their location information. Therefore, the contrastive loss can reflect the patterns between the location and the similarity value to the neural network. Furthermore, the contrastive loss value between the feature maps of the original view and the masked portions in the second view is higher than that of the other sections. As a result, as the loss value for the masked sections increases, there is a corresponding increase in attention toward predicting these areas.

### Loss function

When designing a loss function, there are three key tasks to consider.

**Consistency loss** The first objective of CLLD is extracting visible segments from the input. To train the CNN backbone to produce accurate features, we utilize a  $\mathcal{L}_{const}$  (Eq. (5)), which contrasts the consistency of the feature maps that came out of CNNs for two views (original and masked).

$$\mathcal{L}_{cons} = -\frac{1}{h \times w} \times \sum_{i=1}^h \sum_{j=1}^w \frac{y_{ij} \cdot y'_{ij}}{\|y_{ij}\|_2 \times \|y'_{ij}\|_2} \quad (5)$$

To assess their consistency, we calculate the cosine similarity between each pixel on feature map  $y$  and its corresponding pixel on feature map  $y'$ . A positive cosine similarity value suggests that the features are consistent, while a negative value indicates inconsistency between the features. Therefore we multiply the value by a negative sign to have a positive loss value for the inconsistency. Finally, we compute the average of cosine similarities of all pixels of feature maps.

**Similarity loss** Another objective of CLLD is to train CNNs to predict features for masked areas. To fulfill this objective, we introduce similarity loss  $\mathcal{L}_{sim}$ . The similarity loss (Eq. (6)) computes the consistency between  $CS(y, (\forall p \in y'))$  and  $CS(y', (\forall p \in y))$ .

$$\mathcal{L}_{sim} = -\frac{CS(y, (\forall p \in y')) \cdot CS(y', (\forall p \in y))}{\|CS(y, (\forall p \in y'))\|_2 \times \|CS(y', (\forall p \in y))\|_2} \quad (6)$$

$\mathcal{L}_{sim}$  is the cosine similarity of two cross similarities.  $CS(y, (\forall p \in y'))$  and  $CS(y', (\forall p \in y))$  may be differences in the results due to the presence of masked areas on the feature map  $y'$ . By using cosine similarity, we can identify the



variations between different patches, as shown in Figure 4. This allows us to train our model, using  $\mathcal{L}_{Sim}$ , to predict the masked area by pinpointing the source of inconsistency.

**Classification loss** To learn the categorization representation, we use an instance-level cosine similarity loss  $\mathcal{L}_{inst}$  (Equation Eq. (7)).

$$\mathcal{L}_{inst} = 2 - 2 \frac{\hat{y} \cdot \hat{y}'}{\|\hat{y}\|_2 \times \|\hat{y}'\|_2} \quad (7)$$

where the  $\hat{y}$  and  $\hat{y}'$  are normalized vectors of  $y$  and  $y'$ , respectively.

The loss function we used in this study is the summation of all aforementioned loss functions (Eq. (8)).

$$\mathcal{L}_{clld} = \mathcal{L}_{cons} + \mathcal{L}_{sim} + \mathcal{L}_{inst} \quad (8)$$

## Experimental setup

For a fair comparison, all backbones are pretrained on unlabeled ImageNet-1K (Deng et al. 2009). Our approach is assessed on ResNet50. We evaluate the performance of our self-supervised method on pre-training backbones of three lane detection algorithms: U-Net (Ronneberger, Fischer, and Brox 2015), RESA (Zheng et al. 2021), and CLRNNet (Zheng et al. 2022).

All hyperparameters of the lane detection methods remain unchanged. We use the LARS optimizer with a cosine learning rate, with the starting learning rate set at 1.0. The batch size is 1024, and the weight decay is  $1e-5$ . For the masking, we set  $\rho = 14$ . For the momentum encoder, the momentum value is started from 0.99 and increases to 1. We train ResNet50 on 6 Nvidia<sup>®</sup> A100-40GB GPUs and all the backbones for 100 epochs. To study the effect of  $\alpha$ , we train ResNet50 with three different values of  $\alpha$ : 1, 2, and 3. For these studies, we mask 30% of the original image to make the masked image. We fine-tune all lane detection algorithms on 2 Nvidia<sup>®</sup> RTX A6000.

## Benchmarks

We evaluate CLLD on two popular lane detection benchmarks, CuLane (Pan et al. 2018) and TuSimple (Weng et al. 2021).

**CuLane** CuLane contains 55 hours of video data from highways and urban scenarios. CuLane has nine validation subsets: *Normal*, *Crowd*, *Night*, *Noline*, *Shadow*, *Arrow*, *Hlight*, and *Curve*. Lane marking predictions are shown as 30-pixel wide lines. A true positive prediction has an IoU  $> 0.5$ , while lower values are false positives. No prediction for a labeled ground truth lane is a false negative. False Positives (FP) and False Negatives (FN) are considered unsuccessful predictions. The common metrics used for benchmarking on CuLane are  $Precision = \frac{TP}{TP+FP}$  and  $Recall = \frac{TP}{TP+FN}$ , and  $F1 - measure = \frac{2 \times Precision \times Recall}{Precision + Recall}$ .

**TuSimple** the dataset consists of 3626 videos, each with a resolution of 1280x720 pixels and a length of about 20 seconds, captured from a camera mounted on the windshield of

a vehicle driving on highways in different weather and lighting conditions. The accuracy metric used for benchmarking on TuSimple is  $accuracy = \frac{\sum_{clip} C_{clip}}{\sum_{clip} S_{clip}}$ , where  $C_{clip}$  is the number of predicted points and  $S_{clip}$  is the entire number of lane points on ground truth.

## Results

We specifically chose to evaluate CLLD with U-Net because it is a common encoder-decoder architecture used in various methods that approach lane detection as a segmentation-based problem (Lee and Liu 2022; Zou et al. 2019; Tran and Le 2019a; Moujtahid et al. 2022). In addition, we tested our method using RESA (Zheng et al. 2021), which is currently the state-of-the-art semantic segmentation lane detection method that is not based on the U-Net architecture. This independent validation is necessary to ensure the accuracy of our results. Lastly, we evaluated CLLD using CLRNNet, a leading anchor-based lane detection method.

## Comparison prior works

**U-Net** The results of the lane detection using U-Net with CLLD pretraining, along with comparisons with other contrastive learning methods, are presented in Table 1. More comprehensive results are available in Table 7 in the supplementary material. Results show that CLLD ( $\alpha = 3$ ) outperforms all other methods on TuSimple. Furthermore, all CLLD versions outperform other methods on CuLane according to the most accuracy metrics. PixPro is the only method that provides better precision than CLLD; however, it provides  $\approx 2\%$  lower recall than the average of all CLLD versions. A comparison between CLLD and PixPro reveals that CLLD generates more false positives, while PixPro produces more false negatives. This comparison shows that CLLD is better at extrapolating lanes compared to PixPro, while PixPro is better represented in lane interpolation. It has been observed that all CLLD variants perform better than VICRegL, despite being trained with 200 fewer epochs. This suggests that a method like VICRegL, which can trade off global and local features, may not be the best option for lane detection tasks. Our primary goal is to detect lanes in low visibility conditions. One example of a low visibility scenario is when lane markings are obscured by shadows. As shown in Table 7, CLLD outperforms all other CL methods, resulting in an improvement of at least 7%.

Table 1: Accuracy of U-Net on CuLane and TuSimple with different contrastive learning methods.

Method	# Epoch	CuLane			TuSimple
		Precision	Recall	F1-measure	Accuracy
PixPro (Xie et al. 2021)	100	73.68	67.15	70.27	95.92
VICRegL (Bardes, Ponce, and LeCun 2022)	300	67.75	63.43	65.54	93.58
DenseCL (Wang et al. 2021)	200	63.8	58.4	60.98	96.13
MoCo-V2 (Chen et al. 2020b)	200	63.08	57.74	60.29	96.04
CLLD ( $\alpha = 1$ )	100	71.98	69.2	70.56	95.9
CLLD ( $\alpha = 2$ )	100	70.69	69.36	70.02	95.98
CLLD ( $\alpha = 3$ )	100	71.31	69.59	70.43	96.17

**RESA** Table 2 (Appendix Table 9) illustrates the performance of RESA on CuLane and TuSimple with different contrastive learning methods. Using RESA architecture, all variations of CLLD outperform all other methods.

CLLD ( $\alpha = 1$ ) is the best method with regard to CuLane precision. CLLD ( $\alpha = 3$ ) also outperforms other methods on TuSimple and mostly CuLane according to different evaluation metrics. Similar to U-Net, the combination of RESA and CLLD is markedly ( $\approx 4\%$ ) better on the shadow subset of CuLane which illustrates the generalization of improvements on low visible lane detection.

Table 2: Performance of RESA (Zheng et al. 2021) on CuLane and TuSimple with different contrastive learnings.

Method	# Epoch	CuLane			TuSimple
		Precision	Recall	F1-measure	Accuracy
PixPro (Xie et al. 2021)	100	77.41	73.69	75.51	96.6
VICRegL (Bardes, Ponce, and LeCun 2022)	300	76.27	69.58	72.77	96.18
DenseCL (Wang et al. 2021)	200	77.67	73.51	75.53	96.28
MoCo-V2 (Chen et al. 2020b)	200	78.12	73.36	75.66	96.56
CLLD ( $\alpha = 1$ )	100	79.01	72.99	75.88	96.74
CLLD ( $\alpha = 2$ )	100	78	73.45	75.66	96.78
CLLD ( $\alpha = 3$ )	100	78.34	74.29	76.26	96.81

**CLRNet** Table 3 (Appendix Table 10) presents the effectiveness of CLLD on CLRNet performance. Compared to prior contrastive learning methods, CLLD achieves over 1% improvement on the Recall metric of CuLane. It also achieves state-of-the-art results on TuSimple accuracy and CuLane’s F-Measure. Similar to previous studies, PixPro achieves better Precision on CuLane. Unlike U-Net and RESA, CLRNet does not use a segmentation-based approach to detect lanes. Instead, it identifies lane anchors and connects them to achieve better lane extrapolation. However, when combined with CLLD, CLRNet does not show as much improvement in detecting low visible lanes such as those in shadow sub-data when compared to the other two segmentation-based models. This does not mean that segmentation-based lane detection is outdated as it is more flexible in its detection mechanism, making it a more generalized approach. The results obtained from TuSimple are evidence to support this claim.

Table 3: Performance of CLRNet (Zheng et al. 2022) on CuLane and TuSimple with different pretraining strategies

Method	# Epoch	CuLane			TuSimple
		Precision	Recall	F1-measure	Accuracy
PixPro (Xie et al. 2021)	100	89.19	70.39	78.67	93.88
VICRegL (Bardes, Ponce, and LeCun 2022)	300	87.72	71.15	78.72	89.01
DenseCL (Wang et al. 2021)	200	88.07	69.67	77.8	85.15
MoCo-V2 (Chen et al. 2020b)	200	88.91	71.02	78.96	93.87
CLLD ( $\alpha = 1$ )	100	88.72	71.33	79.09	90.68
CLLD ( $\alpha = 2$ )	100	87.95	71.44	78.84	93.48
CLLD ( $\alpha = 3$ )	100	88.59	71.73	79.27	94.25

### Comparison with supervised learning

Table 4 presents the results of the CLLD pretraining strategy with supervised pretraining. The best improvement ( $\approx 1\%$  in the average of all CuLane subsets), compared to supervised learning, is in the RESA architecture with ResNet50 as the backbone. CLLD also achieves a maximum  $\approx 4\%$  increase in CuLane’s low visible subsets, such as the shadow. CLLD outperforms supervised learning on RESA for all metrics on both datasets, with the exception of the FP rate on TuSimple. False positive is the only metric for which supervised learning has provided better prediction outcomes than CLLD at a rate of 0.0343 per prediction.

CLLD performance is equivalent to supervised learning based on most evaluation metrics on CLRNet ( $\pm \leq 1\%$ ). For the shadow subset of CuLane, the accuracy of CLRNet was about  $\approx 4\%$  better with CLLD pretraining than supervised learning. CLLD performance in U-Net is comparable to supervised learning. It gains over 1% better accuracy than supervised learning with respect to the precision metric. CLLD also produces over 300 more FPs than supervised learning in the cross subset of CuLane.

### Visual demonstration

Figure 5 illustrates a qualitative comparison of lane prediction pretrained on CLLD compared with supervised learning and prior lane detection methods. The results illustrate CLLD performance, especially for the most left lane with an occluder. Most other training strategies detect lanes, but with many false positives, except DenseCL, which destroys the lane. PixPro also has worse predictions than CLLD, with significant false negatives for the occluded part.

Figure 6 is the interpolated view of the latent layer on RESA for supervised and self-supervised learning (CLLD). The results show that supervised learning pays more attention to the texture of the road; however, CLLD focuses more on the shapes of objects and the lane, which is more important for the lane detection task. Wu et al. (Wu et al. 2022) study these differences in supervised and self-supervised learning behavior. This may be a reason why self-supervised learning performs better on the lane detection task.

### Ablation study

**Similarity loss impact** Table 5 (Appendix Table 10) ablates CLLD performance with a single similarity loss, a single consistency loss, and the combination of them together. We did not study the absence of instance loss because it did not affect the segmentation results and used it for classification. The accuracy of combining similarity and grouping is remarkably better than using only one.  $\mathcal{L}_{sim} + \mathcal{L}_{cons}$  performed significantly better results ( $\approx 5\%$ ) in challenging subsets of CuLane dataset such as the shadow; however, the performance in the normal CuLane subset is not affected by the loss of similarity. This observation illustrates the effect of similarity loss on the detection of low visible lanes.

**Impact of masking as the augmentation** Table 6 examines the effect of the masking strategy on overall accuracy. CLLD with masking yields a significantly better recall in CuLane ( $\approx 4\%$ ); however, it achieves a marginally lower precision ( $\approx 0.2\%$ ). It increases the F-measure by an average of  $\approx 2\%$  over all CuLane subsets. The combination with masking also improves the accuracy of TuSimple markedly ( $\approx 1\%$ ).

### Conclusion

Our paper presents a novel self-supervised approach, Contrastive Learning for Lane Detection via cross-similarity (CLLD), designed to enhance the resilience of lane detection models in adverse conditions. CLLD is a multi-task CL that addresses the challenge of detecting obscured lane

Table 4: Comparison of the performance of state-of-the-art lane detection methods on CuLane and TuSimple in two situations of pretraining with supervised learning and CLLD self-supervised learning. For clarification, we also show the performance gain for each model in all parameters.

Method	Pretrain	CuLane												TuSimple		
		Overall(%)			F1-Measure(%)											
		Precision	Recall	F1	Normal	Crowd	Night	Noline	Shadow	Arrow	Hlight	Curve	FP	Accuracy	FP	FN
U-Net (Ronneberger, Fischer, and Brox 2015)	Supervised	70.93	69.65	70.28	89.82	67.72	64.95	40.49	68.13	84.48	59.83	67.02	2482	96.24	0.0489	0.0428
	CLLD	71.31	69.59	70.43	89.8	68.39	64.65	40.68	68.86	84.5	58.93	66.2	2656	96.17	0.055	0.045
RESA(Zheng et al. 2021)	Supervised	77.51	73.15	75.27	92.16	73.16	69.99	47.71	72.97	88.16	68.79	70.65	1503	96.67	0.031	0.0265
	CLLD	78.34	74.29	76.26	92.57	74.35	71.21	48.83	76.62	89.14	67.58	72.68	1454	96.81	0.0343	0.0264
CLRNet(Zheng et al. 2022)	Supervised	88.21	71.88	79.22	93.1	77.83	74.3	52.69	76.92	89.63	73.16	69.41	1082	93.17	0.0232	0.0748
	CLLD	88.59	71.73	79.27	92.94	77.44	74.43	53.3	81.2	89.31	72.46	68.4	1026	94.25	0.214	0.069

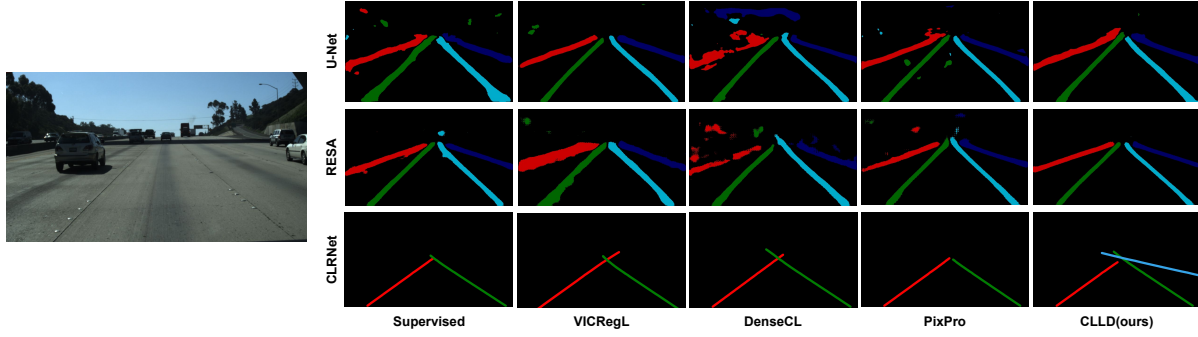


Figure 5: Visualized Results. Comparison of the results of CLLD with prior SSL methods and supervised learning.

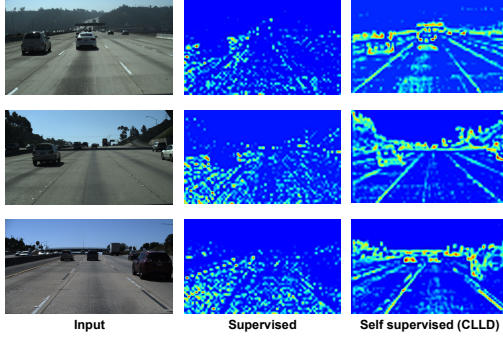


Figure 6: Low-level features in RESA; The left column in the input image, the middle column is low-level features in supervised learning, the right column is low-level features in CLLD.

markings caused by factors like poor lighting and weather by integrating our novel operation cross-similarity to local feature CLs. Our method (CLLD) demonstrates remarkable improvements over existing contrastive learning techniques, particularly excelling in scenarios with low visibility, such as shadows. We tested CLLD for lane detection in real-world scenarios to enhance autonomous driving technology.

Table 5: **Ablation: Multi-task contrastive learning.** Comparison the impact of similarity loss and consistency loss on the lane detection accuracy

$\mathcal{L}_{sim}$	$\mathcal{L}_{cons}$	CuLane			TuSimple
		Precision	Recall	F1	Accuracy
*		76.91	70.82	73.74	95.94
	*	77.41	73.69	75.51	95.92
*	*	78.34	74.29	76.26	96.17

Table 6: **Ablation: Impact of the masking as the augmentation.** Comparison of the accuracy of CLLD with or without using masking as the augmentation

Masking	CuLane			TuSimple
	Precision	Recall	F1	Accuracy
No	72.2	65.77	68.84	95.7
Yes	71.98	69.2	70.56	96.17

## References

- Bao, H.; Dong, L.; Piao, S.; and Wei, F. 2021. BEiT: BERT Pre-Training of Image Transformers. In *International Conference on Learning Representations*.
- Bardes, A.; Ponce, J.; and LeCun, Y. 2021. Vicreg: Variance-invariance-covariance regularization for self-supervised learning. *arXiv preprint arXiv:2105.04906*.
- Bardes, A.; Ponce, J.; and LeCun, Y. 2022. Vicregl: Self-

supervised learning of local visual features. *arXiv preprint arXiv:2210.01571*.

Borkar, A.; Hayes, M.; and Smith, M. T. 2011. A novel lane detection system with efficient ground truth generation. *IEEE Transactions on Intelligent Transportation Systems*, 13(1): 365–374.

Chen, T.; Kornblith, S.; Norouzi, M.; and Hinton, G. 2020a. A simple framework for contrastive learning of visual representations. In *International conference on machine learning*, 1597–1607. PMLR.

Chen, X.; Fan, H.; Girshick, R.; and He, K. 2020b. Improved baselines with momentum contrastive learning. *arXiv preprint arXiv:2003.04297*.

Chen, X.; and He, K. 2021. Exploring simple siamese representation learning. In *Proceedings of the IEEE/CVF Conference on Computer Vision and Pattern Recognition*, 15750–15758.

Chen, X.; Xie, S.; and He, K. 2021. An empirical study of training self-supervised vision transformers. In *Proceedings of the IEEE/CVF International Conference on Computer Vision*, 9640–9649.

Deng, J.; Dong, W.; Socher, R.; Li, L.-J.; Li, K.; and Fei-Fei, L. 2009. Imagenet: A large-scale hierarchical image database. In *2009 IEEE conference on computer vision and pattern recognition*, 248–255. Ieee.

Deusch, H.; Wiest, J.; Reuter, S.; Szczot, M.; Konrad, M.; and Dietmayer, K. 2012. A random finite set approach to multiple lane detection. In *2012 15th International IEEE Conference on Intelligent Transportation Systems*, 270–275. IEEE.

Grill, J.-B.; Strub, F.; Altché, F.; Tallec, C.; Richemond, P.; Buchatskaya, E.; Doersch, C.; Avila Pires, B.; Guo, Z.; Gheshlaghi Azar, M.; Piot, B.; kavukcuoglu, k.; Munos, R.; and Valko, M. 2020. Bootstrap Your Own Latent - A New Approach to Self-Supervised Learning. In Larochelle, H.; Ranzato, M.; Hadsell, R.; Balcan, M.; and Lin, H., eds., *Advances in Neural Information Processing Systems*, volume 33, 21271–21284. Curran Associates, Inc.

Gurghian, A.; Koduri, T.; Bailur, S. V.; Carey, K. J.; and Murali, V. N. 2016. Deeplanes: End-to-end lane position estimation using deep neural networks. In *Proceedings of the IEEE conference on computer vision and pattern recognition workshops*, 38–45.

He, K.; Chen, X.; Xie, S.; Li, Y.; Dollár, P.; and Girshick, R. 2022. Masked autoencoders are scalable vision learners. In *Proceedings of the IEEE/CVF conference on computer vision and pattern recognition*, 16000–16009.

He, K.; Fan, H.; Wu, Y.; Xie, S.; and Girshick, R. 2020. Momentum contrast for unsupervised visual representation learning. In *Proceedings of the IEEE/CVF conference on computer vision and pattern recognition*, 9729–9738.

Henaff, O. 2020. Data-efficient image recognition with contrastive predictive coding. In *International conference on machine learning*, 4182–4192. PMLR.

Hur, J.; Kang, S.-N.; and Seo, S.-W. 2013. Multi-lane detection in urban driving environments using conditional random fields. In *2013 IEEE Intelligent vehicles symposium (IV)*, 1297–1302. IEEE.

Kim, J.; and Lee, M. 2014. Robust lane detection based on convolutional neural network and random sample consensus. In *Neural Information Processing: 21st International Conference, ICONIP 2014, Kuching, Malaysia, November 3-6, 2014. Proceedings, Part I* 21, 454–461. Springer.

Kim, J.; and Park, C. 2017. End-to-end ego lane estimation based on sequential transfer learning for self-driving cars. In *Proceedings of the IEEE conference on computer vision and pattern recognition workshops*, 30–38.

Lee, D.-H.; and Liu, J.-L. 2022. End-to-end deep learning of lane detection and path prediction for real-time autonomous driving. *Signal, Image and Video Processing*, 1–7.

Liu, R.; Yuan, Z.; Liu, T.; and Xiong, Z. 2021. End-to-End Lane Shape Prediction With Transformers. In *Proceedings of the IEEE/CVF Winter Conference on Applications of Computer Vision (WACV)*, 3694–3702.

Mitrovic, J.; McWilliams, B.; Walker, J.; Buesing, L.; and Blundell, C. 2020. Representation learning via invariant causal mechanisms. *arXiv preprint arXiv:2010.07922*.

Moujtahid, S.; Benmokhtar, R.; Breheret, A.; and Boukhdhir, S.-E. 2022. Spatial-unet: Deep learning-based lane detection using fisheye cameras for autonomous driving. In *Image Analysis and Processing-ICIAP 2022: 21st International Conference, Lecce, Italy, May 23–27, 2022, Proceedings, Part II*, 576–586. Springer.

Neven, D.; Brabandere, B. D.; Georgoulis, S.; Proesmans, M.; and Gool, L. V. 2018. Towards End-to-End Lane Detection: an Instance Segmentation Approach. In *2018 IEEE Intelligent Vehicles Symposium (IV)*, 286–291.

Pan, X.; Shi, J.; Luo, P.; Wang, X.; and Tang, X. 2018. Spatial As Deep: Spatial CNN for Traffic Scene Understanding. In *AAAI Conference on Artificial Intelligence (AAAI)*.

Qin, Z.; Zhang, P.; and Li, X. 2022. Ultra fast deep lane detection with hybrid anchor driven ordinal classification. *IEEE Transactions on Pattern Analysis and Machine Intelligence*.

Qu, Z.; Jin, H.; Zhou, Y.; Yang, Z.; and Zhang, W. 2021. Focus on Local: Detecting Lane Marker From Bottom Up via Key Point. In *Proceedings of the IEEE/CVF Conference on Computer Vision and Pattern Recognition (CVPR)*, 14122–14130.

Ronneberger, O.; Fischer, P.; and Brox, T. 2015. U-net: Convolutional networks for biomedical image segmentation. In *Medical Image Computing and Computer-Assisted Intervention-MICCAI 2015: 18th International Conference, Munich, Germany, October 5-9, 2015, Proceedings, Part III* 18, 234–241. Springer.

Sermanet, P.; Eigen, D.; Zhang, X.; Mathieu, M.; Fergus, R.; and LeCun, Y. 2013. Overfeat: Integrated recognition, localization and detection using convolutional networks. *arXiv preprint arXiv:1312.6229*.



- Sun, T.-Y.; Tsai, S.-J.; and Chan, V. 2006. HSI color model based lane-marking detection. In *2006 IEEE Intelligent Transportation Systems Conference*, 1168–1172.
- Tabelini, L.; Berriel, R.; Paixao, T. M.; Badue, C.; De Souza, A. F.; and Oliveira-Santos, T. 2021. Keep Your Eyes on the Lane: Real-Time Attention-Guided Lane Detection. In *Proceedings of the IEEE/CVF Conference on Computer Vision and Pattern Recognition (CVPR)*, 294–302.
- Tian, Y.; Krishnan, D.; and Isola, P. 2020. Contrastive multiview coding. In *Computer Vision—ECCV 2020: 16th European Conference, Glasgow, UK, August 23–28, 2020, Proceedings, Part XI 16*, 776–794. Springer.
- Tran, L.-A.; and Le, M.-H. 2019a. Robust U-Net-based road lane markings detection for autonomous driving. In *2019 International Conference on System Science and Engineering (ICSSE)*, 62–66. IEEE.
- Tran, L.-A.; and Le, M.-H. 2019b. Robust U-Net-based Road Lane Markings Detection for Autonomous Driving. In *2019 International Conference on System Science and Engineering (ICSSE)*, 62–66.
- Wang, J.; Ma, Y.; Huang, S.; Hui, T.; Wang, F.; Qian, C.; and Zhang, T. 2022. A Keypoint-Based Global Association Network for Lane Detection. In *Proceedings of the IEEE/CVF Conference on Computer Vision and Pattern Recognition (CVPR)*, 1392–1401.
- Wang, X.; Zhang, R.; Shen, C.; Kong, T.; and Li, L. 2021. Dense contrastive learning for self-supervised visual pre-training. In *Proceedings of the IEEE/CVF Conference on Computer Vision and Pattern Recognition*, 3024–3033.
- Weng, C.; Wang, W.; Zhou, D.; Cui, S.; Sun, Y.; Liu, X.; and Kweon, I. S. 2021. The TuSimple Benchmark for Autonomous Driving: A Comprehensive Dataset and Baseline. *IEEE Transactions on Pattern Analysis and Machine Intelligence*, 43(1): 285–300.
- Wu, H.; Gao, Y.; Zhang, Y.; Lin, S.; Xie, Y.; Sun, X.; and Li, K. 2022. Self-supervised models are good teaching assistants for vision transformers. In *International Conference on Machine Learning*, 24031–24042. PMLR.
- Wu, P.-C.; Chang, C.-Y.; and Lin, C. H. 2014. Lane-mark extraction for automobiles under complex conditions. *Pattern Recognition*, 47(8): 2756–2767.
- Xiao, T.; Reed, C. J.; Wang, X.; Keutzer, K.; and Darrell, T. 2021. Region similarity representation learning. In *Proceedings of the IEEE/CVF International Conference on Computer Vision*, 10539–10548.
- Xie, Z.; Lin, Y.; Zhang, Z.; Cao, Y.; Lin, S.; and Hu, H. 2021. Propagate Yourself: Exploring Pixel-Level Consistency for Unsupervised Visual Representation Learning. In *Proceedings of the IEEE/CVF Conference on Computer Vision and Pattern Recognition (CVPR)*, 16684–16693.
- Yu, B.; and Jain, A. 1997. Lane boundary detection using a multiresolution Hough transform. In *Proceedings of International Conference on Image Processing*, volume 2, 748–751 vol.2.
- Zhao, X.; Vemulapalli, R.; Mansfield, P. A.; Gong, B.; Green, B.; Shapira, L.; and Wu, Y. 2021. Contrastive learning for label efficient semantic segmentation. In *Proceedings of the IEEE/CVF International Conference on Computer Vision*, 10623–10633.
- Zheng, T.; Fang, H.; Zhang, Y.; Tang, W.; Yang, Z.; Liu, H.; and Cai, D. 2021. Resa: Recurrent feature-shift aggregator for lane detection. In *Proceedings of the AAAI Conference on Artificial Intelligence*, volume 35, 3547–3554.
- Zheng, T.; Huang, Y.; Liu, Y.; Tang, W.; Yang, Z.; Cai, D.; and He, X. 2022. Clnet: Cross layer refinement network for lane detection. In *Proceedings of the IEEE/CVF conference on computer vision and pattern recognition*, 898–907.
- Zou, Q.; Jiang, H.; Dai, Q.; Yue, Y.; Chen, L.; and Wang, Q. 2019. Robust lane detection from continuous driving scenes using deep neural networks. *IEEE transactions on vehicular technology*, 69(1): 41–54.

Table 7: U-Net(Ronneberger, Fischer, and Brox 2015) complete table

Method	Epochs	Backbone	CuLane												TuSimple		
			Overall(%)			F1-Measure(%)									FP		
			Precision	Recall	F1	Normal	Crowd	Night	Noline	Shadow	Arrow	Hlight	Curve	Cross	Accuracy	FP	FN
PixProt(Xie et al. 2021)	100	ResNet50	73.68	67.15	70.27	88.27	68.85	65.54	41.12	57.25	83.17	58.2	66.07	1820	95.92	0.0643	0.052
VICRegL(Bardes, Ponce, and LeCun 2022)	300	ResNet50	67.75	63.43	65.54	85.56	63.63	60.15	35.52	55.54	78.17	50.67	60.47	2673	93.58	0.1427	0.1077
MoCo-V2(Chen et al. 2020b)	200	ResNet50	63.08	57.74	60.29	80.02	61.91	56.51	33.54	53.3	74.42	49.13	61.07	7561	96.13	0.0524	0.047
DenseCL(Wang et al. 2021)	200	ResNet50	63.8	58.4	60.98	80.65	63.01	56.84	35.17	53.98	74.73	48.28	61.5	7784	96.04	0.04742	0.0505
CLLD(ours)( $\alpha = 1$ )	100	ResNet50	71.98	69.2	70.56	89.74	68.23	65.14	40.82	64.72	83.5	59.46	65.62	2112	96.17	0.055	0.045
CLLD(ours)( $\alpha = 2$ )	100	ResNet50	70.69	69.36	70.02	89.29	67.68	64.36	40.04	70.96	83.33	59.93	64.97	2117	95.98	0.0564	0.0488
CLLD(ours)( $\alpha = 3$ )	100	ResNet50	71.31	69.59	70.43	89.8	68.39	64.65	40.68	68.86	84.5	58.93	66.2	2656	95.9	0.0636	0.0515

Table 8: RESA(Zheng et al. 2021) complete table

Pretrain	Epochs	Backbone	CuLane												TuSimple		
			Overall(%)			F1-Measure(%)									FP		
			Precision	Recall	F1	Normal	Crowd	Night	Noline	Shadow	Arrow	Hlight	Curve	Cross	Accuracy	FP	FN
PixProt(Xie et al. 2021)	100	ResNet50	77.41	73.69	75.51	92.78	73.12	70.17	48.72	71.89	89.55	66.68	72.02	1699	96.6	0.0362	0.0298
VICRegL(Bardes, Ponce, and LeCun 2022)	300	ResNet50	76.27	69.58	72.77	90.27	71.56	68.39	44.27	59.88	85.75	63.05	67.75	1933	96.18	0.044	0.041
MoCo-V2(Chen et al. 2020b)	200	ResNet50	78.12	73.36	75.66	92.45	74.19	70.35	47.47	71.27	88.31	69.23	69.12	1471	96.56	0.0341	0.0307
DenseCL(Wang et al. 2021)	200	ResNet50	77.67	73.51	75.53	92.69	73.33	70.51	48.14	70.36	89.03	65.13	70.45	1456	96.28	0.04117	0.04112
CLLD(ours)( $\alpha = 1$ )	100	ResNet50	79.01	72.99	75.88	92.49	74.19	70.8	46.42	75.17	89.15	67.07	70.4	1276	96.74	0.0341	0.0277
CLLD(ours)( $\alpha = 2$ )	100	ResNet50	78	73.45	75.66	92.47	73.85	70.45	47.41	75.88	88.67	65.93	70.28	1584	96.78	0.037	0.0262
CLLD(ours)( $\alpha = 3$ )	100	ResNet50	78.34	74.29	76.26	92.57	74.35	71.21	48.83	76.62	89.14	67.58	72.68	1454	96.81	0.0343	0.0264

Table 9: CLRNNet(Zheng et al. 2022) complete table

Pretrain	Epochs	Backbone	CuLane												TuSimple		
			Overall(%)			F1-Measure(%)									FP		
			Precision	Recall	F1	Normal	Crowd	Night	Noline	Shadow	Arrow	Hlight	Curve	Cross	Accuracy	FP	FN
PixProt(Xie et al. 2021)	100	ResNet50	89.19	70.39	78.67	91.69	77.34	74.45	51.8	80.52	88.26	72.99	68.23	898	93.88	0.0355	0.0667
VICRegL(Bardes, Ponce, and LeCun 2022)	300	ResNet50	87.72	71.15	78.72	92.57	75.94	74.53	52.52	79.45	88.85	73.88	67.57	1070	89.01	0.3115	0.2316
MoCo-V2(Chen et al. 2020b)	200	ResNet50	88.91	71.02	78.96	93	77.35	73.6	51.56	78.91	89.77	71.35	68.61	1011	93.87	0.11276	0.10391
DenseCL(Wang et al. 2021)	200	ResNet50	88.07	69.67	77.8	91.83	75.93	72.97	50.28	77.64	88.39	71.67	67.41	983	85.15	0.1497	0.2714
CLLD(ours)( $\alpha = 1$ )	100	ResNet50	88.72	71.33	79.09	92.85	77.6	74.07	52.39	80.42	89.15	72.29	67.1	989	90.68	0.0217	0.1179
CLLD(ours)( $\alpha = 2$ )	100	ResNet50	87.95	71.44	78.84	92.85	76.93	74.17	51.96	81.02	89.07	72.15	69.5	1186	93.48	0.0352	0.0749
CLLD(ours)( $\alpha = 3$ )	100	ResNet50	88.59	71.73	79.27	92.94	77.44	74.43	53.3	81.2	89.31	72.46	68.4	1026	94.25	0.214	0.069

Table 10: **Ablation: Impact of the loss function.** Comparison of CLLD accuracy with or without using Similarity loss (Complete table)

$\mathcal{L}_{sim}$	$\mathcal{L}_{cons}$	CuLane												TuSimple		
		Overall(%)			F-Measures(%)									FP		
		Precision	Recall	F1	Normal	Crowd	Night	Noline	Shadow	Arrow	Hlight	Curve	Cross	Accuracy	FP	FN
*		76.91	70.82	73.74	91.67	71.21	66.84	46.55	70.56	87.1	66.43	66.75	1571	95.94	0.04521	0.0449
*	*	77.41	73.69	75.51	92.78	73.12	70.17	48.72	71.89	89.55	66.68	72.02	1699	95.92	0.0643	0.052
*	*	78.34	74.29	76.26	92.57	74.35	71.21	48.83	76.62	89.14	67.58	72.68	1454	96.17	0.055	0.045

Table 11: **Ablation: Impact of RandomDrop.** Comparison of CLLD accuracy with or without using RandomDrop as the augmentation (Complete table)

RandomDrop	CuLane												TuSimple		
	Overall(%)			F-Measures(%)									FP		
	Precision	Recall	F1	Normal	Crowd	Night	Noline	Shadow	Arrow	Hlight	Curve	Cross	Accuracy	FP	FN
No	72.2	65.77	68.84	87.34	67.95	63.61	38.37	61.25	81.17	56.41	62.95	2324	95.7	0.0652	0.0554
Yes	71.98	69.2	70.56	89.74	68.23	65.14	40.82	64.72	83.5	59.46	65.62	2112	96.17	0.055	0.045